Journal of Materials Chemistry A

Accepted Manuscript

ROYAL SOCIETY OF CHEMISTRY

www.rsc.org/materialsA

Journal of
Materials Chemistry A

PAPER

A graphene/Co_9S_8 nanocomposite paper as a binder-free and free-standing Anode for Lithium-ion batteries

Received 00th January 20xx,
Accepted 00th January 20xx

DOI: 10.1039/x0xx00000x

www.rsc.org/

Huanhuan Wang,[a] Songtao Lu,[a] Yan Chen,[a] Lu Han,[a] Jia Zhou,[a] Xiaohong Wu,[a*] Wei Qin[b*]

Flexible lithium ion batteries with high energy density have recently received tremendous interest due to their potential applications in flexible electronic devices. Herein, we report a simple high energy ball-milling technique together with vaccum filtration to fabricate a highly flexible, conductive, robust and free-standing RGO/Co_9S_8 nanocomposite paper with high conductivity (121 S/cm), tensile strength (50.4 MPa) and Young's modulus (3.5 GPa) which can be directly used as free-standing anode for flexible LIBs without binders, conducting agents and metallic current collectors. The free-standing RGO/Co_9S_8 anode with high mass active material loading 66.7wt % Co_9S_8 can deliver a high specific capacity of 1415 mAh·g^{-1}_{Co9S8} (944 mAh·$g^{-1}_{electrode}$) and maintain 573 mAh·g^{-1}_{Co9S8} (382.2 mAh·$g^{-1}_{electrode}$) after 500 cycles at a current density of 1C (1C=545 mA·g^{-1}). More importantly, the rate capability was improved by introducing RGO. The RGO/Co_9S_8 anode exhibited impressive capacities of 1096.70 mAhg^{-1}_{Co9S8} with a capacity recuperability of 69.4% as the current returned to 0.1C. These results demonstrate that the well designed nanocomposite is of great potential as the anode for flexible LIBs. As far as we known, Such improved electrochemical performance can be attributed to the nanosized Co_9S_8 particles with a diameter of ~25 nm homogeneously dispersed on the surface of high conductive graphene sheets that can be obtained owing to the milling impact stress, which enhances surface electrochemical reactivity and shortens the transport length of lithium ions and electronics. what's more, the large specific surface area of the graphene sheet enable the uniform distribution of Co_9S_8, better ability to accommodate volume expansion/shrinkage of Co_9S_8 during repeated charge/discharge cycles.

Introduction

The ever increasing demand for the flexible devices, such as liquid crystalline displays (LCDs), organic light-emitting diodes (OLEDs), active ration-frequency identification tags (RFID), wearable sensors, and roll-up displays, has attracted great researchers' interest in the flexible energy systems, especially the flexible lithium ion batteries (LIBs) due to the high energy density and cycle performance.[1-5] However, the related studies are still in the nascent stage and the large-scale use is limited, mainly because of the low capability of fabricating flexible electrodes. In this context, the primary components of flexible LIBs are the electrodes fabricated by coating slurry-typed mixtures of nanostructured active materials on metal strip current collectors, which are mainly aluminum (5 mg/cm^2) and copper (10 mg/cm^2).[6] In recent years, fabricating flexible anodes by depositing metal oxides (SnO_2,[7] Fe_3O_4,[8] TiO_2,[9, 10] etc.) directly on flexible and conductive substrates, such as CNT buckypaper, graphene paper, and non-woven activated carbon fabric (ACF), has shown advanced performance for flexible LIBs due to their high conductivity and flexibility. However, the high capacity is only obtained at a low current density and the rate capability still needs to be improved.[7] Hence, many considerable research attempts have been made to explore new anode materials with high energy density. Among those candidates, Co_9S_8, a transition metal sulfide, has attracted considerable interest because of its high theoretical capacities and low cost.[2, 11, 12] Various Co_9S_8 nanostructures (e.g., mesocrystal Co_9S_8 hollow spheres,[13] rose-like Co_9S_8,[14] cotton-like Co_9S_8 nanoparticles,[12] Co_9S_8 yolk–shell microspheres,[15] and hollow nanospheres of mesoporous Co_9S_8,[16]) have been synthesized and showed improved electrochemical performances compared to the bulk Co_9S_8 owing to the novel nanostructure, which are facile for the diffusion of lithium ions during the charge-discharge process. To achieve high specific capacity and high power density with low cost, a plethora of interest has been paid to the combined usage of carbon[17-19]. most recently, Qian et al. prepared a one-dimensional MWCNT@a-C@Co_9S_8 nanocomposite as anode for LIBs,[20] owing to the crystalline Co_9S_8 nanoparticles sit on the MWCNT@a-C nanotubes, it exhibited a capacity of 662 mAh·g^{-1} after 120 cycles at a current density of 1 A·g^{-1}. However, there is nearly no report on fabricating of flexible Co_9S_8 anode to the best of our knowledge. More importantly, the electrochemical performance of the state-of-the-art Co_9S_8 anode is so poor that its commercial application is hindered, the poor electrochemical performance of the Co_9S_8 anode is caused by the intrinsically low electronic conductivity of Co_9S_8,[21-24] and the relatively large volume variation of Co_9S_8 during charge/discharge processes.[25-27]

[a]Department of Chemistry, Harbin Institute of Technology, Harbin, Heilongjiang. 150001, PR China. E-mail: wuxiaohong@hit.edu.cn; Fax: +86 451 86402522; Tel: +86 451 86402522
[b]School of Materials Science and Engineering, Harbin Institute of Technology, Harbin, Heilongjiang. 150001, PR China. E-mail: qinwei@hit.edu.cn
Electronic Supplementary Information (ESI) available: [details of any supplementary information available should be included here]. See DOI: 10.1039/x0xx00000x

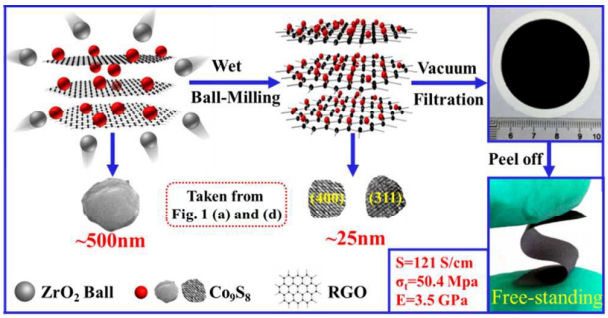

Scheme. 1 Schematic illustration of the fabricated flexible and conductive paper using RGO/Co_9S_8.

Graphene with unique properties including large surface area, low weight, high electrical conductivity, and superior mechanical flexibility, is a promising material in flexible lithium ion batteries.[28-30] Therefore, it is anticipated that graphene will play a great role in the research of flexible RGO/Co_9S_8 anodes due to its triple functions in enhancing electronic conductivity and increasing the mechanical property.

Herein, we present a flexible and robust RGO/Co_9S_8 paper anode for lithium ion batteries with excellent electrochemical performance based on the uniformly dispersed Co_9S_8 particles with a diameter of ~25 nm on the surface of high conductive graphene sheets. The detailed synthetic procedures are shown in Scheme. 1. Typically, Co_9S_8 particles with a diameter of ~500 nm were prepared by ball milling Co and sulfur. The obtained Co_9S_8 particles were dispersed in a homogeneous graphene suspension (water-phase) under ultrasonic conditions. Then, the graphene-Co_9S_8 was ball milled for another 6 hours to further reduce the diameter of Co_9S_8. After vacuum filtration and drying, the graphene/Co_9S_8 paper can be directly used as the electrode without binders, conducting agents and metallic current collectors.

In our approach (Scheme. 2), graphene will be mainly used to increase the conductivity and mechanical properties, thus improve its electrochemical performance and accommodate volume expansion/shrinkage during repeated charge/discharge cycles. Such synergetic effect[31-33] between graphene and nanosized Co_9S_8 will enhance surface electrochemical reactivity and shorten the transport length of lithium ions and electronics, improving the electrochemical performance of RGO/Co_9S_8 paper electrode.[34, 35] As a result, the obtained flexible and robust RGO/Co_9S_8 paper electrode with high Co_9S_8 content (66.7wt %) can deliver a high specific capacity of 1415 $mAh\cdot g^{-1}_{Co9S8}$ (944 $mAh\cdot g^{-1}_{electrode}$) and maintain 573 $mAh\cdot g^{-1}_{Co9S8}$ (382.2 $mAh\cdot g^{-1}_{electrode}$) after 500 cycles at a current density of 1C (1C=545 $mA\cdot g^{-1}$), demonstrating comparable electrochemical properties with others' reports. (Table S1).[13, 16, 20, 36, 37]

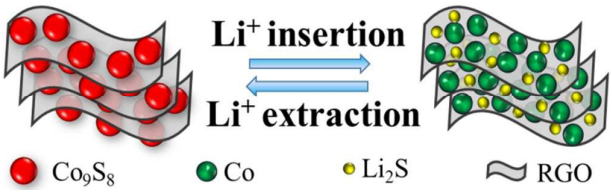

Scheme. 2 The Schematic illustration of Li^+ insertion/extraction processes of RGO/Co_9S_8 nanocomposite.

Experimental

Preparation of Co_9S_8

Co_9S_8 compound was prepared using a high energy ball mill (FRITSCH PULVERISETTE-7) according to our previous work.[38]

Preparation of graphene oxide (GO)

The graphene oxide was prepared from natural flake graphite through typical Hummer's method.[39] The concentration of the GO suspension obtained was 1.0 mg/ml, which was determined by drying 40 mL of the suspension at 60 °C under vacuum for 1 week and then weighing the dried GO.

Preparation of reduced graphene oxide (RGO)

RGO was synthesized using hydrazine hydrate as a reducing agent.[40] Typically, 40ml GO suspension (C=1.0mg/ml), hydrazine hydrate (20 ul, wt%=80%, ρ=1.03g/cm^3) and Ammonium hydroxide (140 ul) was added into an airtight container (100 ml capacity). The mixture was kept at 90°C for 1 hour, then washed with deionized water for several times after cooled to room temperature. Finally dried by vacuum freeze-drying and the concentration of the RGO suspension can be obtained (0.74mg/ml).

Preparation of RGO/Co_9S_8 nanocomposite

Various RGO/Co_9S_8 nanocomposites with different weight ratios of RGO to Co_9S_8 were prepared by ball milling appropriate amount of Co_9S_8 in the as-prepared RGO suspension in a ZrO_2 vessel at a speed of 700 rpm for 6h under Ar gas atmosphere with a ball to powder weight ratio of 15:1. After that, the RGO/Co_9S_8 nanocomposite was collected by vacuum filtration, and could form freestanding papers. The whole process is shown in Scheme. 1.

Materials Characterization

The crystal structures of the samples were carried out on an X-ray diffractometer (XRD, Rigaku D/max IIIA). Morphology of the Co_9S_8 and RGO/Co_9S_8 paper was investigated by field-emission scanning electron microscopy (FESEM, JSM-6700) and transmission electron microscopy (TEM, FEI, Tecnai G^{2}S-Twin). Raman spectra were obtained by using a Bruker Optics Senterra R200-L Raman scattering microscope with a laser wave length of 663nm. Electronic conductivity of samples was measured using Hall Effect Measurement System (Swim HALL8800, Chinese Taipei) at room temperature. The mechanical properties of samples were measured by a commercial nanotensile testing system (Nano UTMTM Universal Testing System T150, Agilent Technologies).

Evaluation of Electrochemical Properties

The Co_9S_8 working electrodes were prepared by mixing 70wt% of Co_9S_8 powder, 20wt% of acetylene black, and 10wt% of polyvinylidene difluoride binder in N-methyl-2-pyrrolidone (NMP) solvent to form homogenous slurry. The slurries were spread on copper foil substrates, and the coated electrodes were pressed after being dried in a vacuum oven at 100℃ for 24h. The as-fabricated RGO/Co_9S_8 nanocomposite papers were directly used as the cathode in the electrochemical performance test. CR 2032-type coin cells used in the above two kinds of as-prepared electrodes were assembled in an Ar-filled glove box with lithium foil as the anode under the concentrations of

moisture and oxygen below 1ppm. The electrolyte used was 1M $LiPF_6$ in ethylene carbonate (EC)/diethyl carbonate (DEC) (1:1 in volume), Microporous polypropylene paper (Celgard 2400) was used as the cell separator. The electrochemical properties of anodes were evaluated by a galvanostatic discharge/charge technique performed using a NEWARE battery tester at different current rates with a voltage window of 0.01-3.0V (vs Li^+/Li). Electrochemical impedance spectra measurements were performed under an electrochemical workstation (PARSTAT 4000, Princeton, U.S.A) on single cells under different discharge states from 100KHz to 100mHz.

Results and discussion

SEM image of the pristine Co_9S_8 shown in Fig. 1(a), the as-prepared Co_9S_8 with a large size of ~500nm, which is very similar to our previous results.[38] After ball milling the Co_9S_8 in graphene suspension, the diameter can be reduced to ~25nm because of the impacts from the powerful ball-collisions during the process would direct these particles together at collision points, where the collision-induced energy triggers and/or facilitates the formation of the ultra-fine size for the Co_9S_8 particles.[41] The aqueous environment is benefit for homogeneous distribution of these Co_9S_8 nanoparticles on the surface of the graphene sheets, forming graphene/Co_9S_8 nanocomposite finally, as shown in Fig. 1(b). The corresponding selected-area electron diffraction (SAED) of the nanocomposite (Fig. 1c) displays a series of bright concentric rings, all of which could be indexed as cubic-phase Co_9S_8, which is consistent with the XRD results. The HRTEM image further indicates that the crystalline Co_9S_8 nanoparticles dispersed on the graphene substrate. As exhibited in Fig. 1(d), the lattice spacing of 0.300nm, 0.248nm, correspond to the

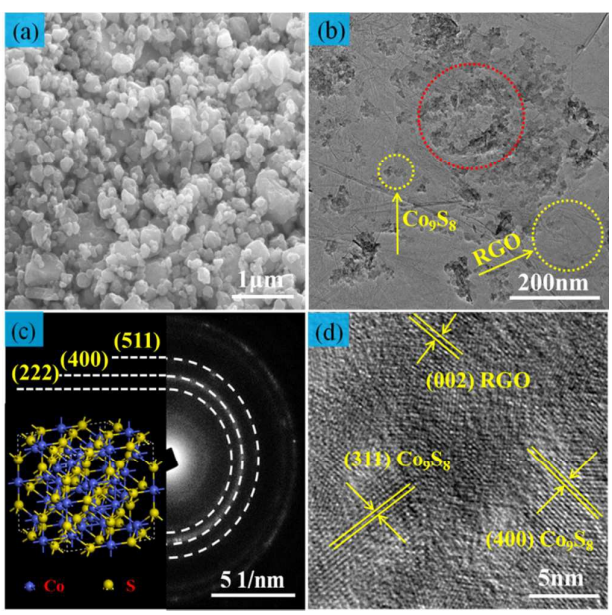

Fig. 1 (a) SEM image of Co_9S_8; (b) TEM image of RGO/Co_9S_8 nanocomposite; (c) and (d) are respectively Selected area electron diffraction (SAED) pattern (the right half), crystal structure image of the resulting Co_9S_8 (the left half) and HRTEM image of the RGO/Co_9S_8 nanocomposite marked by the red circle in (b).

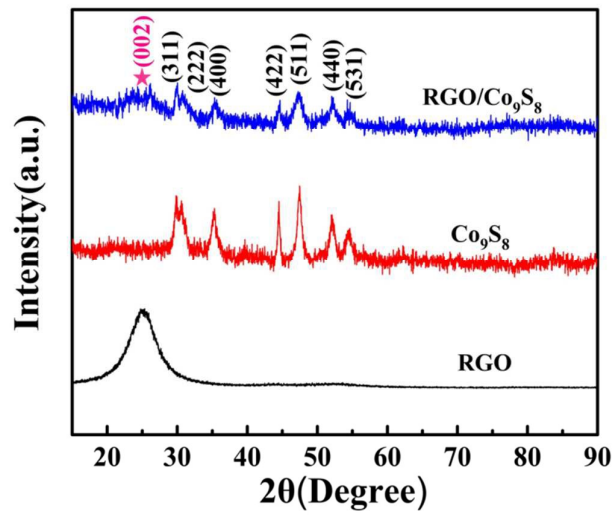

Fig. 2 XRD patterns of pristine Co_9S_8, RGO and RGO/Co_9S_8 nanocomposite.

(311), (400) planes of cubic Co_9S_8 and the d-spacing at 0.34nm agree well with those from (002) planes of graphene.[20] Moreover, the EDX elemental mapping of the RGO/Co_9S_8 nanocomposite (Fig.S1.) confirmed uniform distribution of Co_9S_8 nanoparticles on the RGO matrix.

X-ray powder diffraction (XRD) was tested to study the crystal structure of RGO/Co_9S_8 nanocomposite, and the result is shown in Fig. 2, All the reflection peaks appeared in the as-prepared Co_9S_8 could be exclusively attributed to Co_9S_8 (PDF# 02-1459) with the pure fcc structure in space group Fm3m (225). After high energy ball milling at 700 rpm under Ar atmosphere for 6 hours, the XRD pattern of the RGO/Co_9S_8 nanocomposite shows that diffraction peaks corresponding to Co_9S_8 are significantly broadened. This broadening is attributed to the decrease of the crystalline grain size and the increase of the lattices train during the milling process with the extension of ball milling time and high ball milling speed.[41-43] In addition, a very weak and broad peak related to RGO was also observed in the case of the nanocomposite at $2\theta = 25.3°$ can be attributed to graphite-like (002) structure.[44, 45] According to the XRD results, the grain size of the Co_9S_8 in RGO/Co_9S_8 is 20-50nm calculated by Scherrer equation ($D_{(hlk)} = K\lambda/B_{1/2}\cos\theta$), in good agreement with the HRTEM image of the RGO/Co_9S_8 nanocomposite.

The evolution of the structure during the ball-milling process of RGO/Co_9S_8 nanocomposite is investigated by Raman spectroscopy (Fig.3). The Raman spectra of RGO/Co_9S_8 nanocomposite can be divided into two parts: <1000 cm^{-1} and >1000 cm^{-1}. A few strong Raman bands (<1000 cm^{-1}) could be indexed to Co_9S_8 appeared in the spectrum.[46, 47] The Raman bands after 1000 cm^{-1} are indexed to RGO. It is well known that the pronounced D band at 1353.97cm^{-1} is a disordered band associated with structural defects, amorphous carbon or edges that can break the symmetry and selection rule, and the G band at 1596.49cm^{-1} is assigned to the first-order scattering of the E_{2g} mode observed for sp^2 carbon domains.[48, 49] after ball milling at a speed of 700rpm for 6h, the D/G intensity ratio of the RGO

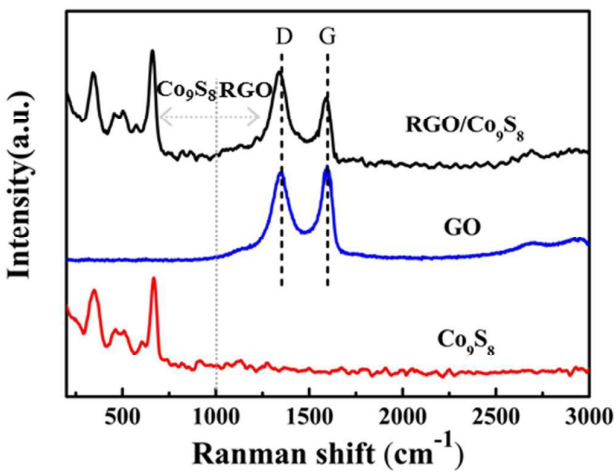

Fig. 3 Raman spectra of pure Co_9S_8, GO and RGO/Co_9S_8 nanocomposite for comparisons.

at a speed of 700rpm for 6h, the D/G intensity ratio of the RGO in the RGO/Co_9S_8 nanocomposite increased obviously compared to that of pure GO (from 0.96 to 1.09), indicating the content of the activated carbon atoms in graphene structure from disorder, edges and defects is increased after the high energy ball milling process due to the embedding of Co_9S_8 under mechanical milling impact stress, which is further confirmed by the negatively shift of the D band and G band to 1348.36 and 1590.49cm^{-1} respectively.[50] To summarize, the changes occurring during chemical reduction and high energy ball milling treatment give indication of the properties of RGO/Co_9S_8 nanocomposite depending on the natures of carbon, that is to say, a large amount of the structural defects in RGO are beneficial for the improvement of electrochemical performance.

The mechanical properties and electrochemical properties were tested in order to optimize the weight ratio of Co_9S_8 in the nanocomposites, and the results were shown in Fig. S2 and S3. As a result, the mechanical properties of the RGO/Co_9S_8 paper decreased with the increasing amount of Co_9S_8. More importantly, when the weight ratio of Co_9S_8 is 66.7 w t%, the RGO/Co_9S_8 paper with electronic conductivity of 121 S/cm, Young's modulus of 3.5 G Pa and tensile strength of 50.4 MPa displayed the highest reversible capacity. Thus it was selected as the material studied further. Fig. 4(a) compares the 1st, 2nd, 10th charge/discharge profiles of cathodes assembled with or without the incorporation of RGO at a current density of 1C within a voltage window of 0.01-3.0 V vs. Li^+/Li at room temperature, respectively. Three voltage plateaus at ~1.25V, ~1.0V and ~0.75 V were clearly observed during the discharge process for RGO/Co_9S_8 nanocomposite, which is agree well with others' reports.[13, 18] The plateaus at ~1.25V and ~1.0V can be attributed to the reaction:[12, 51, 52] $Co_9S_8 + 16Li^+ + 16e \leftrightarrow 8Li_2S + 9Co$. And the voltage flat at ~0.75V is ascribed to the decomposition of the electrolyte and the formation of solid electrolyte interface (SEI) film on RGO surface. During the charge process, three plateaus at about ~1.07 V, ~1.25V, and ~2.20V were observed. Potentials at ~1.25V, and ~2.20V were due to the conversation of Co to Co_9S_8.[53] And the plateau at 1.07V can be ascribed to the electrochemical delithiation of RGO. The RGO/Co_9S_8 nanocomposite could deliver a high initial capacity of 1415 $mAh\cdot g^{-1}_{Co9S8}$ (944 $mAh\cdot g^{-1}_{electrode}$) with a low Coulombic efficiency of 65% in the first cycle (Fig. 4b). The low Coulombic efficiency is due to the irreversible processes, including the electrolyte decomposition, the formation of SEI film, the trapping of lithium inside the active material, or Li-ion reaction with unreduced functional groups on graphene.[54-58] More importantly, the Coulombic efficiency of RGO/Co_9S_8 quickly approaches ~100%, indicating high charge/discharge reversibility of the RGO/Co_9S_8 electrode. On the other hand, the control electrode made with Co_9S_8 without graphene exhibited inferior stability. In this case, the electrode was able to deliver an initial discharge capacity of 816.26 $mAh\cdot g^{-1}_{Co9S8}$ (571.38 $mAh\cdot g^{-1}_{electrode}$).

With continued cycling, as shown in Fig. S4, the electrode exhibited well-overlapped and flat plateaus, suggesting good stability and reversibility of the electrode. On the basis of the discharge results, as shown in Fig. 4b and 4c, the flexible RGO/Co_9S_8 nanocomposite paper was able to deliver 573 $mAh\cdot g^{-1}_{Co9S8}$ (382.2 $mAh\cdot g^{-1}_{electrode}$) after 500 cycles, which is substantially higher than that of bare Co_9S_8 particles, demonstrating improved capacity by graphene. The improved reversible capacity and long cycle stability can be contributed to the uniform distribution of the nanosized Co_9S_8 on the high conductive graphene sheets with significantly mechanical properties, and it will not only short the transport length of both the electron and lithium ions but also accommodate volume expansion/shrinkage during repeated charge/discharge cycles. In order to investigate the structure stability of RGO/Co_9S_8, the coin cells after 500 cycles were disassembled in argon-filled glove box and washed several times with dimethyl carbonate (DMC) to remove soluble species for the SEM observation. And the result was shown in Fig. S5, indicating its significant ability of structural preservation.

Electrochemical impedance spectra (EIS) measurements were performed to gain better understanding of the improved electrochemical performance of the RGO incorporation. Fig. S6 gives the Nyquist plots for electrodes after 500 cycles, showing a depressed semicircle at the high-to-medium frequencies connected to a slope at the low frequencies, which are associated to the charge transfer resistance (R_{ct}) and the ion diffusion inside the electrode, respectively. The R_{ct} value of cell assembled using RGO/Co_9S_8 nanocomposite electrode (13.5 Ω) is approximately two times lower than that of the cell assembled without RGO (28.6Ω). The result confirms that RGO can enhance the electrical conductivity, lowering the internal resistance of the cell. As a result, the kinetic of electrochemical lithium insertion/extraction was improved, endowing the RGO/Co_9S_8 nanocomposite electrode with high reversible capacity.

The rate capability of the RGO/Co_9S_8 nanocomposite and Co_9S_8 electrodes were studied by repeated charge-discharge tests conducted at increasing current densities from 0.1 to 2 C, and the results are compared in Fig. 4(d). The RGO/Co_9S_8 delivered a reversible specific capacity of 1580.78, 1068.14, 987.12, 895.80, and 807.63$mAh\cdot g^{-1}_{Co9S8}$ at 0.1C, 0.2C, 0.5C,

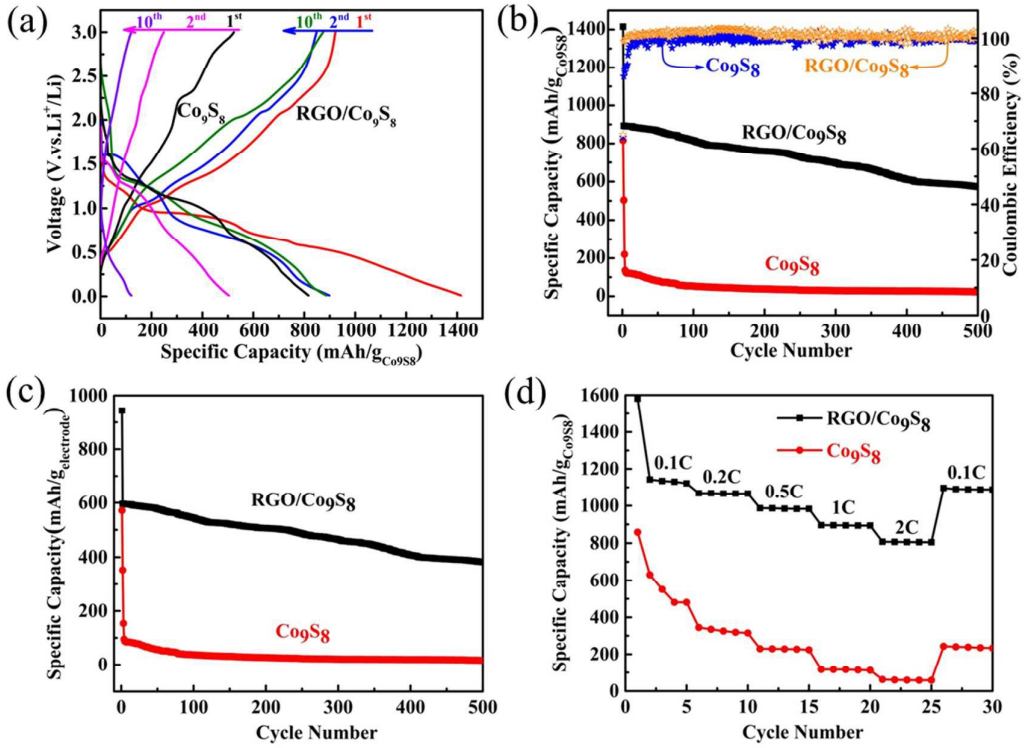

Fig. 4 Comparison of (a) the 1st, 2nd, 10th charge-discharge voltage profiles; (b) the capacity based on the Co_9S_8 weight as a function of cycle numbers and the Coulombic efficiency; (c) the capacity based on the cathode weight (including the conductive additive and binder) as a function of cycle numbers; and (d) Rate capacity at different current densities of RGO/Co_9S_8 paper and Co_9S_8 particles.

1C, and 2C. In strong contrast, the Co_9S_8 exhibited much worse rate performance at the same condition, delivering a specific capacity of 858.22, 345.01, 230.20, 116.92, and 62.6mAh·g^{-1}_{Co9S8}, respectively. Moreover, the specific capacities of RGO/Co_9S_8 nanocomposite electrode can recover to 1096.7 mAh·g^{-1}_{Co9S8} when the rate returned to the initial 0.1C after 25 cycles, giving a capacity recuperability of 69.4% which is much higher than that of Co_9S_8 (28.3%). It is evidently demonstrated that RGO/Co_9S_8 nanocomposite exhibits higher reversible capacity, better rate capability and excellent cyclic stability in comparison with Co_9S_8 electrode.

Conclusions

In conclusion, we have designed and prepared a highly flexible, robust, and conductive paper anode based on nanostructural RGO/Co_9S_8 nanocomposite for LIBs. Owing to the uniform distribution of Co_9S_8 nanoparticles on graphene that can improve the conductivity and accommodate volume expansion/shrinkage, this free-standing RGO/Co_9S_8 paper with a high tensile strength of 50.4 MPa can deliver a highly initial discharge capacity of 1415 mAh·g^{-1}_{Co9S8} (944 mAh·$g^{-1}_{electrode}$) and still maintain a reversible capacity of 573 mAh·g^{-1}_{Co9S8} (382.2 mAh·$g^{-1}_{electrode}$) even after 500 cycles at a current density of 1C (1C=545 mA·g^{-1}). These results suggest that the design of graphene with active materials to form the robust and flexible paper brings new opportunities to construct the free-standing electrode for wearable and lightweight energy storage devices with high energy density.

Acknowledgements

This work was supported by the National Natural Science Foundation of China (Nos. 51173033, 51572060 and 51502062), the Fundamental Research Funds for the Central Universities (No.HIT.BRETIII.201224 and 201312) and Program for Innovation Research of Science in Harbin Institute of Technology (PIRS of HIT-No. 201506). Excellent Youth Foundation of Heilongjiang Scientific Committee (No.JC2015010)

Notes and references

1. Q. Cheng, Z. Song, T. Ma, B. B. Smith, R. Tang, H. Yu, H. Jiang and C. K. Chan, *Nano Lett.*, 2013, **13**, 4969-4974.
2. J. B. Goodenough and Y. Kim, *Chem. Mater.*, 2010, **22**, 587-603.
3. S. Song, S. W. Kim, D. J. Lee, Y. G. Lee, K. M. Kim, C. H. Kim, J. K. Park, Y. M. Lee and K. Y. Cho, *ACS Appl. Mater. Interfaces,* 2014, **6**, 11544-11549.
4. M. Armand and J. M. Tarascon, *Nature*, 2008, **451**, 652-657.
5. G. Zhou, F. Li, and H. M. Cheng, *Energy Environ. Sci.*, 2014, **7**, 1307-1338.
6. L. B. Hu, H. Wu, F. L. Mantia, Y. Yuan and Y. Cui, *ACS Nano*, 2010, **4**, 5843-5848.

7. D. H. Wang, R. Kou, D. W. Choi, Z. G. Yang, Z. M. Nie, D. H. Hu, J. G. Zhang, J. Liu, Michael A. Pope and I. A. Aksay, *ACS Nano*, 2010, **4**, 1587-1595.
8. Y. Wu, Y. Wei, J. Wang, K. Jiang and S. Fan, *Nano Lett.*, 2013, **13**, 818-823.
9. S. Liu, Z. Wang, C. Yu, H. B. Wu, G. Wang, Q. Dong, J. Qiu, A. Eychmuller and X. W. David Lou, *Adv Mater*, 2013, **25**, 3462-3467.
10. H. M. Ren, Y. H. Ding, F. H. Chang, X. He, J. Q. Feng, C. F. Wang, Y. Jiang and P. Zhang, *Appl. Surf. Sci.*, 2012, **263**, 54-57.
11. V. Etacheri, R. Marom, R. Elazari, G. Salitra and D. Aurbach, *Energy Environ. Sci.*, 2011, **4**, 3243-3262.
12. J. Wang, S. H. Ng, G. X. Wang, J. Chen, L. Zhao, Y. Chen and H. K. Liu, *J. Power Sources*, 2006, **159**, 287-290.
13. R. C. Jin, J. Zhou, Y. Guan, H. Liu and G. Chen, *J. Mater. Chem. A*, 2014, **2**, 13241-13244.
14. R. C. Jin, J. Liu, Y. Xu, G. Li and G. Chen, *J. Mater. Chem. A*, 2013, **1**, 7995-7999.
15. Y. N. Ko, S. H. Choi, S. B. Park and Y. C. Kang, *Chem. Asian J.*, 2014, **9**, 572-576.
16. Y. L. Zhou, D. Yan, H. Y. Xu, J. K. Feng, X. L. Jiang, J. Yue, J. Yang, and Y. T. Qian, *Nano Energy*, 2015, **12**, 528-537.
17. J. Guo, F. Li, Y. Sun, X. Zhang and L. Tang, *Electrochim. Acta*, 2015, **167**, 32-38.
18. G. Huang, T. Chen, Z. Wang, K. Chang and W. Chen, *J. Power Sources*, 2013, **235**, 122-128.
19. Z. Li, W. Li, H. Xue, W. Kang, X. Yang, M. Sun, Y. Tang and C. S. Lee, *RSC Adv.*, 2014, **4**, 37180-37186.
20. Y. L. Zhou, D. Yan, H. Y. Xu, S. Liu, J. Yang and Y. T. Qian, *Nanoscale*, 2015, **7**, 3520-3525.
21. S. Amaresh, K. Karthikeyan, I. C. Jang and Y. S. Lee, *J. Mater. Chem. A*, 2014, **2**, 11099-11106.
22. H. Chen, J. Jiang, L. Zhang, H. Wan, T. Qi and D. Xia, *Nanoscale*, 2013, **5**, 8879-8883.
23. H. Chen, J. Jiang, L. Zhang, D. Xia, Y. Zhao, D. Guo, T. Qi and H. Wan, *J. Power Sources*, 2014, **254**, 249-257.
24. M. He, L. X. Yuan and Y. H. Huang, *RSC Adv.*, 2013, **3**, 3374-3383.
25. K. Brezesinski, J. Haetge, J. Wang, S. Mascotto, C. Reitz, A. Rein, S. H. Tolbert, J. Perlich, B. Dunn and T. Brezesinski, *Small*, 2011, **7**, 407-414.
26. M. He, L. Yuan, X. Hu, W. Zhang, J. Shu and Y. Huang, *Nanoscale*, 2013, **5**, 3298-3305.
27. J. X. Zhu, Z. Y. Yin, D. Yang, T. Sun, H. Yu, H. E. Hoster, H. H. Hng, H. Zhang and Q. Y. Yan, *Energy Environ.Sci.*, 2013, **6**, 987-993.
28. T. Hu, X. Sun, H. Sun, M. Yu, F. Lu, C. Liu and J. Lian, *Carbon*, 2013, **51**, 322-326.
29. J. W. Lee, S. Y. Lim, H. M. Jeong, T. H. Hwang, J. K. Kang and J. W. Choi, *Energy Environ.Sci.*, 2012, **5**, 9889-9894.
30. N. Li, G. Zhou, R. Fang, F. Li and H. M. Cheng, *Nanoscale*, 2013, **5**, 7780-7784.
31. Q. Wang, J. Sun, Q. Wang, D. A. Zhang, L. L. Xing and X. Y. Xue, *J. Mater. Chem. A*, 2015, **3**, 5083-5091.
32. Q. Wang, D. A. Zhang, Q. Wang, J. Sun, L. L. Xing and X. Y. Xue, *Electrochim. Acta*, 2014, **146**, 411-418.
33. D. A. Zhang, Q. Wang, Q. Wang, J. Sun, L. L. Xing and X. Y. Xue, *Electrochim. Acta*, 2015, **173**, 476-482.
34. P. Poizot, S. Laruelle, S. Grugeon, L. Dupont and J. M. Tarascon, *Nature*, 2000, **407**, 496-499.
35. C. Z. Wu, Y. Xie, L. Y. Lei, S. Q. Hu and C. Z. OuYang, *Adv. Mater.*, 2006, **18**, 1727-1732.
36. Y. X. Zhou, H. B. Yao, Y. Wang, H. L. Liu, M. R. Gao, P. K. Shen and S. H. Yu, *Chem.Eur.J.*, 2010, **16**, 12000-12007.
37. W. Shi, J. Zhu, X. Rui, X. Cao, C. Chen, H. Zhang, H. H. Hng and Q. Yan, *ACS Appl. Mater. Interfaces*, 2012, **4**, 2999-3006.
38. W. Qin, B. G. Hu, D. Bao and P. Gao, *Int. J. Hydrogen Energy*, 2014, **39**, 9300-9306.
39. J. P. Zhao, S. F. Pei, W. C. Ren, L. B. Gao, and H. M Cheng, *ACS Nano*, 2010, **4**, 5245-5252.
40. D. Li, M. B. Müller. S. Gilje, Richard B. Kaner, Gordon G. Wallace, *Nat Nanotechnol,* 2008, **3**, 101-105.
41. S. Li, M. Ling, J. Qiu, J. Han and S. Zhang, *J. Mater. Chem. A*, 2015, **3**, 9700-9706.
42. X. Hou, M. Zhang, J. Wang, S. Hu, X. Liu and Z. Shao, *J. Alloys Compd.*, 2015, **639**, 27-35.
43. J. T. Xu, J. L. Shui, J. L. Wang, M. Wang, H. K Liu, S. X. Dou, I. Y. Jeon, J. M. Seo, J. B. Baek. and L. M. Dai, *ACS Nano*, 2014, **8**, 10920–10930.
44. J. Fu, C. Wei, W. Wang, J. L. Wei and J. Lv, *Mater. Res. Innovations*, 2015, **19**, S1-277-S271-280.
45. D. Zhang, X. Zhang, X. Sun, H. Zhang, C. Wang and Y. Ma, *Electrochim. Acta*, 2013, **109**, 874-880.
46. P. F. Yin, L. L. Sun, Y. L. Gao and S. Y. Wang, *Bull. Mater. Sci.*, 2008, **31**, 593-596.
47. L. L. Feng, G. D. Li, Y. Liu, Y. Wu, H. Chen, Y. Wang, Y. C. Zou, D. Wang and X. Zou, *ACS Appl. Mater. Interfaces*, 2015, **7**, 980-988.
48. D. Kim, S. J. Yang, Y. S. Kim, H. Jung and C. R. Park, *Carbon*, 2012, **50**, 3229-3232.
49. S. F. Pei and H. M. Cheng, *Carbon*, 2012, **50**, 3210-3228.
50. A. Bagri, C. Mattevi, M. Acik, Y. J. Chabal, M. Chhowalla and V. B. Shenoy, *Nature Chem.*, 2010, **2**, 581-587.
51. J. L. Gómez-Cámer, F. Martin, J. Morales and L. Sanchez, *J. Electrochem. Soc*, 2008, **155**, A189-A195.
52. A. Débart, L. Dupont, R. Patrice and J. M. Tarascon, *Solid State Sci.*, 2006, **8**, 640-651.
53. X. Fang, X. Yu, S. Liao, Y. Shi, Y. S. Hu, Z. Wang, G. D. Stucky and L. Chen, *Microporous Mesoporous Mater.*, 2012, **151**, 418-423.
54. S. H. Lee, Y. H. Kim, R. Deshpande, P. A. Parilla, E. Whitney, D. T. Gillaspie, K. M. Jones, A. H. Mahan, S. B. Zhang and A. C. Dillon, *Adv. Mater.*, 2008, **20**, 3627-3632.
55. X. H. Liu and J. Y. Huang, *Energy Environ. Sci.*, 2011, **4**, 3844-3860.
56. Y. Mao, Q. Y. Kong, B. K. Guo, X. P. Fang, X. W. Guo, L. Shen, M. Armand, Z. X. Wang and L. Q. Chen, *Energy Environ. Sci.*, 2011, **4**, 3442-3447.
57. Z. Wang, J. S. Chen, T. Zhu, S. Madhavi and X. W. Lou, *Chem. Commun*, 2010, **46**, 6906-6908.
58. J. X. Zhu, T. Zhu, X. Z. Zhou, Y. Y. Zhang, X. W. Lou, X. D. Chen, H. Zhang, H. H. Hng and Q. Y. Yan, *Nanoscale*, 2011, **3**, 1084-1089.